

Pre/post-monsoon Bay of Bengal Tropical Cyclones intensity: role of air-sea coupling and large-scale background state

S. Neetu¹, M. Lengaigne^{2,3}, J. Vialard², G. Samson^{2,4}, S. Masson², K.S. Krishnamohan², I. Suresh¹

¹ CSIR-National Institute of Oceanography (NIO), Goa, India

² LOCEAN-IPSL, Sorbonne Universités (UPMC, Univ. Paris 06)-CNRS-IRD-MNHN, Paris, France

³ Indo-French Cell for Water Sciences, IISc-NIO-IITM-IRD Joint International Laboratory, NIO, Goa, India

⁴ Mercator Océan, Ramonville-Saint-Agne, France

Corresponding author:

S. Neetu

Physical Oceanography Division

National Institute Of Oceanography

Dona Paula - Goa - 403004 India

Email: neetu@nio.org

Key points

- Bay of Bengal tropical cyclones are stronger before than after the monsoon, due to more favorable large-scale background conditions
- Air-sea coupling alleviates the effect of large-scale background conditions, by inhibiting pre-monsoon tropical cyclones
- The air-sea coupling negative feedback on tropical cyclones is weak after the monsoon, due to a fresher, less thermally stratified Bay of Bengal

Abstract:

The densely populated Bay of Bengal (BoB) rim witnesses the deadliest tropical cyclones (TCs) globally, before and after the summer monsoon. Previous studies indicated that enhanced salinity and reduced thermal stratification reduce cooling under BoB TCs after the monsoon, suggesting that air-sea coupling may favor stronger TCs during that season. Using observations and simulations from a $\frac{1}{4}^\circ$ regional ocean-atmosphere model, we show that BoB TCs are stronger before the monsoon due to a more favorable large-scale background state (less vertical wind shear, higher Sea Surface Temperature). Air-sea coupling however alleviates this background state influence, by reducing the number of pre-monsoon intense TCs, because of larger cooling and reduced upward enthalpy fluxes below TCs during that season. As the impact of air-sea interactions on BoB TCs is largest for intense TCs, it should be further investigated for category 3 and above TCs, which are not reproduced at $\frac{1}{4}^\circ$ resolution.

Plain language summary:

Tropical cyclones that develop in the Bay of Bengal are amongst the most lethal globally, owing to the dense and vulnerable coastal population living along its rim. These cyclones mostly occur in April-May and October-December, i.e. before and after the Indian summer monsoon. In this study, we show that there are more intense cyclones before than after the monsoon, because of more favorable large-scale background conditions. We however also show that more intense interactions between the cyclone and the ocean tend to reduce risks for intense cyclones before the monsoon, hence opposing the effect of background conditions. Since air-sea coupling clearly contributes to the Bay of Bengal cyclones intensity, in particular before the monsoon, it should be accounted for in operational forecasts.

1. Introduction

Tropical Cyclones (TCs) are the most devastating natural disasters in coastal regions (Pielke et al., 2008; Blake et al., 2011). Although the Bay of Bengal (BoB) accounts for only 5% of TCs globally, its rim gathers 80% of TC-induced fatalities worldwide (Needham et al., 2015). The category-3 Bhola TC in November 1970 was for instance the deadliest cyclone in the recent history, killing ~500,000 people in Bangladesh (Madsen and Jakobsen, 2004; Islam et al., 2011). The BoB rim is particularly vulnerable to TCs because of its densely-populated low-lying areas and a very shallow continental shelf that amplifies storm surges (up to 14 m; Jakobsen et al., 2006). This exposure to coastal flooding is expected to further increase over the coming decades due to more numerous extreme TCs and rising sea-level associated with climate change (e.g. Karim and Mimura, 2008). These tremendous socio-economical implications call for a better understanding of the mechanisms of TCs intensification in the BoB, in order to improve TCs intensity operational forecasts and projected changes in a warming world.

TCs mostly occur over the southwestern BoB (Figure 1a), with a clear seasonality characterized by a double peak during the pre- (April-May) and post-monsoon (October-December) (Figure 1b). The post-monsoon exhibits a larger TCs density (~ 18 TCs.days.year⁻¹) than the pre-monsoon (~ 11 TCs.days.year⁻¹), with very few events during the rest of the year (Figure 1b). This distinct bimodal distribution is attributed to seasonal changes in the main large-scale environmental parameters that affect TCs development. Large vertical wind shear is a long-known cause for suppressing TCs, and has been underlined as a major player for the absence of TCs during the southwest monsoon (Yanase et al., 2012; Xing and Huang, 2013; Li et al. 2013). Li et al. (2013) however stressed out that the decreased absolute vorticity and Sea Surface Temperature (SST) during the monsoon also contribute to suppress TCs during the monsoon (a colder SST reduces the TC maximum potential intensity; e.g. Emanuel, 1986). On the other hand, the mid-tropospheric humidity increase during the monsoon would tend to favor more TCs, offsetting the effect of the vertical shear, vorticity and SST changes (Li et al., 2013).

While the above-studies have mostly focused on changes in large-scale environmental parameters, some studies have argued that seasonal changes in oceanic stratification may also matter, by influencing air-sea interactions below TCs. TCs cool the ocean under their passage, mostly through vertical mixing (e.g. Price, 1981; Vincent et al., 2012a). This cooling feedbacks negatively on the TCs intensity, since the colder SST reduces the upward enthalpy fluxes that allow TCs to intensify (e.g. Schade, 2000; Cione and Ulhorn, 2003). In the BoB, this TC-induced cooling is three times larger before than after the monsoon, for a given TC strength (Sengupta et al., 2008; Neetu et

al., 2012). Neetu et al. (2012) attributed this to the seasonal changes in the upper ocean stratification between the pre- and post-monsoon. The post-monsoon indeed both displays a stronger salinity stratification (due to the large freshwater flux into the Bay during and shortly after the monsoon; Shenoi et al., 2002; Chaitanya et al., 2014; Akhil et al., 2014) and a deeper thermocline along the BoB rim (in response to coastal Kelvin waves originating from the equatorial region; McCreary et al., 1996) than the pre-monsoon. Balaguru et al. (2012) have underlined that TCs that travel over a strong salinity stratification tend to be associated with weaker cold wakes, stronger upward enthalpy fluxes and stronger intensification rates. Sengupta et al. (2008) have more specifically shown that BoB TCs yield a weaker cold wake after the monsoon, and wondered whether this should favor more intense TCs by reducing the negative feedback due to air-sea coupling. Observations however indicate stronger TCs before the monsoon (Figure 2a; Yanase et al., 2012; Li et al., 2013), hence calling for a more detailed investigation in order to ascertain whether the negative feedback on BoB TCs is indeed weaker after the monsoon.

In a recent study, Lengaigne et al. (2018) investigated the influence of air-sea coupling on TCs characteristics in both hemispheres of the Indian Ocean, comparing a $1/4^\circ$ regional coupled ocean-atmosphere model 20-year-long simulation with a twin forced atmospheric experiment. They found that coupling reduces the number of TCs and their intensity in both hemispheres, as the TC-induced cooling reduces the upward enthalpy fluxes under TCs. They further found that this reduction was particularly large for the northern Indian Ocean most intense TCs, due to higher ambient surface temperatures and larger TC-induced cooling there. Lengaigne et al. (2018) hence suggests that air-sea coupling is very efficient in modulating northern Indian Ocean TCs intensity. They did however not investigate if air-sea coupling allowed stronger post-monsoon TCs due to seasonal changes in ocean stratification, as hinted by Sengupta et al. (2008) and Balaguru et al. (2012).

While a couple of previous studies did investigate the effect of atmospheric parameters on Bay of Bengal pre- and post-monsoon cyclones (e.g. Li et al. 2013; Yanase et al. 2012), they did not examine the effect of air-sea coupling in detail. The present study aims at providing an in-depth analysis of the pre/post monsoon differences in air-sea coupling below TCs and the underlying mechanisms. More specifically, we quantify the respective influences of large-scale background conditions and air-sea coupling on the pre- and post-monsoon BoB TCs intensity distribution using the same set of coupled and forced experiments as in Lengaigne et al. (2018). Considering the effect of air-sea coupling and large-scale background state together will allow to understand why stronger TCs occur *before* the monsoon, while previous studies (Sengupta et al. 2008; Neetu et al. 2012) hint

toward air-sea coupling favoring stronger cyclones *after* the monsoon. The paper is organized as follows. Section 2 summarizes the modeling framework and observed datasets. Section 3 assesses the impact of large-scale background conditions and air-sea coupling on BoB TCs intensity. A discussion of our results against relevant literature is provided in Section 4.

2. Dataset and methods

We use an Indian Ocean [25.5°E-142.5°E, 34.5°S-26°N] configuration of the NOW (NEMO-OASIS3-WRF) regional coupled model at $\frac{1}{4}^\circ$ horizontal resolution. NOW couples the NEMO (Nucleus for European Modeling of the Ocean) ocean component (Madec et al., 2008) to the WRF (Weather Research and Forecasting Model) atmospheric component (Skamarock and Klemp, 2008) through the OASIS3 coupler (Valcke, 2013). This configuration has been extensively described and validated in Samson et al. (2014) and Lengaigne et al. (2018). We therefore only provide a brief summary here. The ocean component has 46 vertical levels, with an enhanced 5 m resolution in the upper ocean. The atmospheric component has 28 sigma vertical levels, with a higher resolution of 30m near the surface and use the updated Kain-Fritsch atmospheric convective scheme (Kain, 2004). Lateral boundary conditions are respectively supplied from a global simulation forced by the Drakkar dataset (Brodeau et al., 2010) for NEMO and from the European Centre for Medium-Range Weather Forecasts ERA-Interim reanalysis (Dee et al., 2011) at 6 hourly for WRF.

We use the same twin-experimental setup as in Lengaigne et al. (2018). A 21-year coupled simulation (CPL) is first performed using the above 1989–2009 lateral boundary conditions. To isolate the effect of air-sea coupling on TCs, an uncoupled atmospheric simulation (FOR) is performed with the same atmospheric boundary conditions as CPL, but forced by SST from the CPL experiment, from which TC-induced cold wakes have been suppressed (see Lengaigne et al., 2018 for details). As a result, the FOR simulation does not account for any oceanic feedback on TCs. The two experiments have a very similar atmospheric background state over the BoB, in particular for variables that have a well-documented influence on TCs (supporting information Figure S1), so that the TCs differences between the two experiments are dominated by the effects of air-sea coupling (also see Lengaigne et al., 2018). Due to chaotic nature of the atmosphere, the small perturbations induced by the removal of TCs cold wakes yield different TCs tracks between the FOR and CPL simulations. While individual TCs tracks are different in the two simulations, we will examine statistical differences in e.g. the number of cyclones, or cyclone intensity distribution in the rest of the paper. Lengaigne et al. (2018) indeed demonstrated that comparing the statistics of simulated TCs in these twin experiments allows diagnosing the influence of air-sea coupling on TCs.

The first year of each experiment is discarded: the simulations are hence analyzed over a 20-years period. TCs from both simulations are tracked using the same methodology as in Samson et al. (2014) and Lengaigne et al. (2018) using criteria similar to those considered in previous studies (Jourdain et al., 2011; Jullien et al., 2014):

- 10 m wind $> 17.5 \text{ m}\cdot\text{s}^{-1}$ associated with a local minimum in sea-level pressure.
- 850 hPa vorticity $> 3 \times 10^{-4} \text{ s}^{-1}$ $[\text{SEP}]$
- 700–300 hPa mean temperature anomaly $> 1^\circ\text{K}$.

TCs are defined as sustained 10-m winds more than $17.5 \text{ m}\cdot\text{s}^{-1}$ and TCs intensities are classified using the Saffir-Simpson scale. TCs temperature anomalies are calculated with respect to their large-scale environment: the TC region is defined as within 3 radii of maximum wind (RMW) around TC center, while the environmental temperature is averaged between 6 and 9 RMW. TC tracks shorter than 1 day are eliminated.

The large-scale background control on TC intensification is assessed by analyzing the three major parameters known to influence TCs intensification in the BoB (Yanase et al., 2012; Li et al., 2013; Xing and Huang, 2013): the vertical wind shear between 850 and 200 hPa in $\text{m}\cdot\text{s}^{-1}$ (SHEAR), the mid-tropospheric relative humidity at 600 hPa (RH) and the maximum potential intensity (MPI; calculated using a routine available at <http://emanuel.mit.edu/products> and closely related to SST, with high SSTs favoring larger MPIs). Following Knaff et al. (2005; 2009) and Neetu et al. (2017), RH and SHEAR are averaged over an annual region within 200–800 km from the center of the storm. This averaging accounts for the fact that environmental parameters can influence the storm far away from its centre, while excluding TC signals close to the TC centre. These parameters are calculated over 1990–2009 from simulations and from the ERA-Interim atmospheric re-analysis (Dee et al., 2011). Observed TCs positions and magnitudes are derived from the International Best Track Archive for Climate Stewardship (IBTrACS; Knapp et al., 2010). Observed SST response under TCs are characterized using a blend of Tropical Rainfall Measuring Mission Microwave Image and advanced Microwave Scanning Radiometer SST data (available from http://www.ssmi.com/sst/microwave_oi_sst_data_description.html) as in Neetu et al. (2012) and Vincent et al. (2012ab).

3. Results

We first assess the ability of the reference coupled model simulation (CPL) to reproduce the main seasonal characteristics of BoB TCs. In observations, the two TC-prone periods (defined as

months with more than 5% of the annual average TC-day count) are April-May and October-December (Figure 1b), and we will use those definitions in the following for the pre- and post-monsoon seasons. In line with observations, the model also displays a clear bimodal TCs seasonal distribution, with few TCs from January to March and during the core of the summer monsoon (July-August). The model seasonal TCs distribution in the BoB however displays some systematic biases compared to observations, including an overestimation of TCs occurrence during the summer monsoon (June-September) and an underestimation in November-December. All the results in this study remain qualitatively similar if the pre- and post-monsoon seasons are rather defined based on the model seasonal TCs distribution (e.g. April-June and September-December). Aside the bimodal seasonal distribution, the CPL experiment is also able to reproduce TCs spatial distribution very well (0.94 pattern correlation between observation and CPL; Figure 1a). As already mentioned in previous papers (Samson et al., 2014; Lengaigne et al., 2018), the model however strongly overestimates cyclogenesis in the BoB, with an average $11.1 \text{ TCs}\cdot\text{year}^{-1}$ compared to $3.2 \text{ TCs}\cdot\text{year}^{-1}$ in observations. We will discuss the potential implications of our model biases in Section 4.

We will now assess how the CPL experiment captures salient features of the observed BoB TC-induced cooling, especially their pre- and post-monsoon amplitude difference. Figure 1cd displays pre- and post-monsoon composites of the cooling under TCs in observations and the CPL simulation. In agreement with previous results (Sengupta et al., 2008; Neetu et al., 2012), the observed BoB TC-induced cooling is on average two to three times larger before (up to -1.3°C ; Figure 1c) than after the monsoon (up to -0.5°C ; Figure 1b). The CPL simulation accurately captures the timing and seasonal contrast of the SST response to TCs, with a weaker cooling during the post- (up to -0.4°C) than during the pre-monsoon (up to -1.3°C). Neetu et al. (2012) attributed this behavior to stronger upper ocean stratification during the post-monsoon. In agreement with their analyses (their Figure 9), the SST response in CPL simulation is larger during the pre-monsoon than during the post-monsoon for a given amount of energy transferred to the ocean by a TC (Figure S2ab in the supporting information), indicating that the pre-monsoon oceanic stratification favors a larger cooling through vertical mixing (Vincent et al., 2012b; Neetu et al., 2012). The “cooling inhibition index”, a proxy of the oceanic resistance to mixing-induced cooling (Vincent et al., 2012a, more details in the supporting information), is indeed higher during the post-monsoon in CPL, in good agreement with observations (Figure S2cd), associated with a stronger salinity and weaker thermal stratification (Figure S3).

We finally assess how the CPL experiment captures the BoB pre- and post-monsoon TCs intensity distributions (Figure 2ab). In line with previous studies (Yanase et al., 2012; Li et al.,

2013), Figure 2a indicates that observed TCs are stronger before than after the monsoon. The CPL simulation reproduces this seasonal contrast, with a larger proportion of strong (Cat-2 and above) TCs before than after the monsoon (8% vs. 2% in the model, 17% vs. 8% in observations). Due to the limited sample size, this difference is only significant at the 84% level in observations while the larger model sample (due to the overestimated model TCs occurrence rate) yields a 99% significance. While there are TCs up to Cat-5 in observations, the model rarely simulates TCs above Cat-2. As acknowledged in other studies using coupled models with a similar spatial resolution in other basins (e.g. Ogata et al., 2015; Jullien et al., 2014), this inability to simulate the most intense TCs is likely related to the relatively coarse horizontal resolution of our atmospheric component ($1/4^\circ$): an atmospheric resolution below 10 km is indeed needed to represent the most intense TCs (Jung et al., 2012; Manganello et al., 2012; Satoh et al., 2012; Murakami et al., 2015).

Despite some shortcomings, the CPL simulation reproduces the BoB TCs spatial and seasonal distribution reasonably well, including the larger cooling under TCs and more intense TCs before the monsoon. This allows us to investigate the relative roles of air-sea coupling and large-scale background parameters in controlling the pre/post-monsoon TC intensity contrasts in this model. Pre-monsoon TCs are stronger despite a more intense cooling, in both observations and the CPL experiment. This indicates that, if air-sea coupling plays any role in the pre-post monsoon TC intensity contrasts, it is not the dominant factor. The FOR simulation also confirms that by exhibiting stronger TCs before the monsoon (Figure 2c). This indicates that the large-scale background state is the main factor that yields more intense TCs before the monsoon.

The pre- minus post-monsoon differences of the most important large-scale background parameters affecting TCs intensification in the BoB are further analyzed on Figure 3a. Large MPI, mid-tropospheric RH and weak SHEAR are favorable to TCs intensification (Merrill, 1988; DeMaria and Kaplan, 1994). The pre-/post-monsoon changes in MPI, RH and SHEAR are very consistent in CPL, FOR and in observations. The seasonal changes in these three environmental parameters favor more intense TCs before the monsoon: ~10% higher MPI, ~10-15% higher RH and ~18% lower SHEAR. The most likely cause for stronger pre-monsoon cyclones are thus the larger MPI, more humid mid-troposphere and weaker vertical wind shear during that season. However note that the effect of tropospheric humidity is not robust as it depends on the averaging strategy to produce Figure 3a, as we will discuss in section 4. The increase in MPI is related to ~1.2°C warmer SST before the monsoon, in both observations and the model.

While the analyses above indicate that large-scale changes dominate the pre-/post-monsoon changes in TC intensity, this does not imply that air-sea coupling does not affect the BoB TCs

intensities. The effect of air-sea coupling on the TCs intensity changes between pre- and post-monsoon can be isolated by comparing the TCs statistical properties in the CPL and FOR twin experiments. Air-sea coupling under TCs does not affect the BoB TC spatial distribution, but slightly reduces the overall frequency of occurrence of TCs (Figures 1a and S3a), as already documented in Lengaigne et al. (2018). This reduction is in particular a bit more prominent during the southwest monsoon, yielding a slightly more realistic bimodal seasonal distribution in CPL than in FOR (Figures 1b and S3b).

Let us now investigate the pre/post monsoon contrasts in air-sea coupling under TCs. The larger oceanic cooling before the monsoon (Figure 1cd) is indicative of a stronger air-sea coupling negative feedback on TC intensity before the monsoon. Figure 3b displays the percentage of intense TCs (Cat-2 and above) during the pre- and post-monsoon for the CPL and FOR experiments. Air-sea coupling yields a much larger reduction of the simulated intense TCs proportion before than after the monsoon. This suggests a strong negative feedback of air-sea coupling on TCs before the monsoon, while this effect is weaker after the monsoon. The effect of air-sea coupling is hence to reduce the intensity of pre-monsoon TCs. This effect is however offset by the stronger impact of changes in MPI, RH and SHEAR, which all tend to induce stronger pre-monsoon TCs.

Figure 4 displays FOR and CPL TCs composites of SST, upward enthalpy fluxes (i.e. the source of energy feeding TCs) and intensification rate under pre- and post-monsoon intensifying TCs as a function of the TC intensity. There is a decrease of the intensification rate for strongest TCs in FOR, both before and after the monsoon, which is simply due to the fact that very strong TCs rarely further intensify. In FOR, the differences between the pre- and post-monsoon TCs intensity are entirely due to environmental parameters, i.e. the weaker vertical shear, more humid troposphere and warmer SST (Figure 3a) before the monsoon. The warmer pre-monsoon SST is also visible in Figure 4a. Those more favorable environmental parameters yield a larger intensification rate for most TCs, especially the most intense (Figure 4c). Warmer SSTs before the monsoon (Figure 4a) induce stronger evaporation rates and upward latent heat fluxes for a given wind intensity (Figure 4b), due to the exponential dependence of saturation vapor pressure on SST in the Clausius-Clapeyron relation. This provides a physical explanation for the process by which the higher MPI yields more TC intensification before the monsoon (Figure 3).

The most relevant large-scale parameters for BoB TCs intensification are almost identical in CPL and FOR simulations (Figure 3a, supporting information Figure S1), so that the TCs differences between those simulations can be attributed to the effect of air-sea coupling under TCs. Composite maps indicate an average cooling of up to -1.2°C under TCs during the pre-monsoon, which is

strongly reduced during the post monsoon (Figures S5f and S6f). Echoing this, the upward enthalpy flux is much more reduced by coupling before (up to -180 Wm^{-2}) than after (up to -100 Wm^{-2}) the monsoon (Figures S5i and S6i). This larger pre-monsoon cooling under TCs offsets the warmer large-scale temperatures. This results in a much weaker difference between pre- minus post-monsoon SST under TCs, especially for the strongest simulated TCs (Figure 4d). As a result, the inner-core upward enthalpy fluxes are strongly reduced by air-sea coupling during the pre-monsoon, and match those during the post-monsoon (Figure 4e). Consequently, TCs intensification rates are reduced during the pre-monsoon (Figure 4f), especially for strongest TCs (wind speed $> 35 \text{ m.s}^{-1}$). Air-sea coupling hence significantly contributes to reduce the number of pre-monsoon intense TCs (Figures 3b, 4c and 4f). After the monsoon, the impact of coupling on TCs intensification rates, and hence intensities, is weaker (Figure 3b, 4c and 4f).

4. Conclusion & Discussion

Based on 8 TCs cases, Sengupta et al. (2008) showed that the strong post-monsoon BoB haline stratification inhibits cooling under TCs. This should hence favore more intense post monsoon TCs, owing to a reduction of the negative feedback associated with air-sea coupling under TCs. Here, we use a regional coupled model to investigate whether this is indeed the case. Our coupled and forced simulations confirm that air-sea coupling reduces the pre-monsoon TCs intensity, as stronger TC cold wakes reduce the upward enthalpy fluxes, leading to weaker intensification rates. This negative effect of air-sea coupling on TCs intensity is however offset by the stronger positive effect of seasonal changes in large-scale environmental parameters. In line with Li et al. (2013), TCs are indeed more intense before than after the monsoon in our model and observations, and those more intense pre-monsoon TCs can be traced back to a warmer ocean (and thus higher MPI), more humid mid-troposphere and weaker vertical shear before than after the monsoon. By quantifying the relative effects of air-sea coupling and large-scale background conditions, our study thus reconciles previous studies suggesting a weaker effect of air-sea coupling after the monsoon (e.g. Sengupta et al. 2008) with observations of stronger cyclones before the monsoon (e.g. Li et al. 2013).

While the effect of air-sea coupling on pre/post monsoon TC intensity contrast is weaker than that of environmental parameters, it is far from negligible, especially before the monsoon when the percentage of strong TCs (Cat-2 and above) exhibits a drop from 23% in the forced simulation to 7% in the coupled one. An important implication of our result is that the operational TCs forecasts for the northern Indian Ocean should include an oceanic component.

Let us now discuss our results against those of Li et al. (2013). First, Li et al. (2013) suggested

higher background RH after than before the monsoon, in contrast to our result. Supporting information Figure S7 demonstrates that the pre minus post monsoon RH is sensitive to whether land values are considered or not. The role of MPI and shear in favoring more intense pre-monsoon TCs is however robust. Li et al. (2013) also partly attributed the more intense observed pre-monsoon TCs to a greater oceanic heat content (OHC) during that season. Supporting information Figure S8 demonstrates that the OHC is indeed higher *before* the monsoon in the model and observations, but that the cooling inhibition of Vincent et al. (2012b) – which tracks the effect of changes in salinity stratification and in the top of the thermocline better – is higher *after* the monsoon, in relation with both thermal and haline stratification changes (Neetu et al. 2012).

Another factor that can influence the TC intensity is the TC translational speed. Slower TCs, for instance, contribute to enhance the effect of air-sea coupling as they induce larger cooling, and also feel the effect of this cooling longer. TCs translation speeds are very similar in the forced and coupled runs, and cannot explain differences between the two. The pre/post monsoon differences in TC translation speed are also small in both model experiments and observations, and are hence unlikely to play any strong role.

The robustness of our results should be assessed in other coupled models. While the overestimated TCs count in our model strengthen the statistical significance of our results, it also suggests that the cumulus parameterization we use (Kain-Fritsch; Kain, 2004) may be overly active and/or too easily triggered by the environmental forcing when the atmospheric column is destabilized, as already discussed in Samson et al. (2014). We tried to assess the robustness of our results by analyzing similar twin experiments using the Bett-Miller-Janjic convective parameterization (Janjic, 1994). This parameterization leads to a more realistic number of TCs in the BoB (Samson et al., 2014), but unfortunately fails to simulate TCs stronger than Cat-1, preventing a meaningful assessment of the impact of air-sea coupling on TCs intensity. However, the fact that Lengaigne et al. (2018) showed that these two parameterizations yield to qualitatively similar results about the air-sea coupling influence on TCs characteristics, including a reduction in the TCs count, is re-assuring. Air-sea coupling indeed reduces the number of TCs more with the Bett-Miller-Janjic parameterisation (65%) than with the Kain-Fritsch scheme (20%; Lengaigne et al., 2018). This suggests an even stronger sensitivity of TCs to air-sea coupling with a different convective scheme to the one used here.

Finally, irrespective of the convective parameterization, our $\frac{1}{4}^\circ$ atmospheric model resolution is not sufficient to simulate the strongest observed TCs as this resolution smoothens out the sharp eyewall structure of tangential winds (Gentry and Lackmann, 2010). Numerous studies using similar

horizontal resolutions in their atmospheric models reported similar issues (e.g. Jullien et al., 2014; Ogata et al., 2015). This is problematic, as our results points to a far larger impact of air-sea coupling on the strongest simulated TCs in the BoB (above 35 m.s⁻¹ maximum winds, Figure 4cf) and because these TCs have the most devastating impacts. A number of studies reported that a 10-km or finer resolution is needed to allow simulating to the most intense TCs (Jung et al., 2012; Manganello et al. 2012; Satoh et al., 2012; Murakami et al., 2015). This study will have to be pursued at such finer resolution. It is for instance likely that the effect of air-sea coupling will be larger at higher resolution. It is also possible that air-sea coupling also contributes to the characteristics of the most intense post-monsoon TCs, as those cyclones are probably strong enough to break through the haline stratification and produce a significant cooling.

Acknowledgments. The authors thank IFCPAR (Indo French Centre for Promotion of Advanced Research), New Delhi for funding of the proposal 4907-1. We also thank IRD (Institut de Recherche pour le Développement) for the financial support of the Indo-French collaboration on Indian Ocean research. I. Suresh acknowledges financial support from the CNES AltiKa project. This is NIO contribution number xxxx. The data relevant to this manuscript are available at https://www.dropbox.com/sh/4kfkuntwxyy19se/AAD9To-kRG_M8A2bqYmr1fwua?dl=0

References

- Akhil, V.P., F. Durand, M. Lengaigne, J. Vialard, M. G. Keerthi, V. V. Gopalakrishna, C. Deltel, F. Papa, and C. de Boyer Montégut (2014), A modeling study of the processes of surface salinity seasonal cycle in the Bay of Bengal, *J. Geophys. Res. Oceans*, 119, 3926–3947, doi:10.1002/2013JC009632.
- Balaguru, K., P. Chang, R. Saravanan, L. R. Leung, Z. Xu, M. Li, and J.-S. Hsieh (2012), Ocean barrier layers' effect on tropical cyclone intensification, *PNAS*, 109, 36, 14343–14347, doi:10.1073/pnas.1201364109.
- Blake, E.S., C.W. Landsea, and E.J. Gibney (2011), The Deadliest, Costliest, and Most Intense United States Tropical Cyclones From 1851 to 2010 (and other Frequently Requested Hurricane Facts). NOAA Technical Memorandum NWS NHC-6. Miami, FL: National Oceanic and Atmospheric Administration, National Weather Service, National HurricaneCenter.
- Brodeau, L., B. Barnier, A.-M. Treguier, T. Penduff, and S. Gulev (2010), An ERA40-based atmospheric forcing for global ocean circulation models, *Ocean Model.*, 31, 3-4, 88-104, doi:10.1016/j.ocemod.2009.10.005.
- Chaitanya V. S., M. Lengaigne, J. Vialard, V. V. Gopalakrishna, F. Durand, C. KranthiKumar, S. Amritash, V. Suneel, F. Papa, and M. Ravichandran (2014), Salinity Measurements Collected by Fishermen Reveal a “River in the Sea” Flowing Along the Eastern Coast of India, *Bull. Amer. Meteor. Soc.*, 95, 1897-1908, doi:10.1175/BAMS-D-12-00243.1.

- Cione JJ, Uhlhorn EW (2003) Sea surface temperature variability in hurricanes: implications with respect to intensity change. *Mon Weather Rev* 131:1783–1796
- Dee, D. P., S. M. Uppala, A. J. Simmons et al. (2011), The ERA-Interim reanalysis: Configuration and performance of the data assimilation system, *Q. J. Roy. Meteorol. Soc.*, 137, 656, 553–597.
- DeMaria M. and J. Kaplan (1994), A statistical hurricane intensity prediction scheme (SHIPS) for the Atlantic basin, *Wea. Forecasting*, 9, 209–220.
- Emanuel KA (1986) An air–sea interaction theory for tropical cyclones. Part 1: steady-state maintenance. *J Atmos Sci* 43:585–604. [https://doi.org/10.1175/1520-0469\(1986\)043<0585:AAS ITF>2.0.CO;2](https://doi.org/10.1175/1520-0469(1986)043<0585:AAS ITF>2.0.CO;2)
- Gentry MS, Lackmann G (2010) Sensitivity of simulated tropical cyclone structure and intensity to horizontal resolution. *Mon Weather Rev* 138:688–704. <https://doi.org/10.1175/2009MWR2976.1>
- Islam, S. M. T., and Z. Chik (2011), Disaster in Bangladesh and management with advanced information system. *Disaster Prev. Manage*, 20, 5, 521–530.
- Jakobsen, F., and M. H. Azam (2006), Cyclone storm surge levels along the Bangladeshi coastline in 1876 and 1960–2000, *Coast Eng. J.*, 48, 3, 295–307.
- Janjic' ZI (1994) The step-mountain eta coordinate model: further developments of the convection, viscous sublayer, and turbulence closure schemes. *Mon Weather Rev* 122:927–945. [https://doi.org/10.1175/1520-0493\(1994\)122<0927:TSMECM>2.0.CO;2](https://doi.org/10.1175/1520-0493(1994)122<0927:TSMECM>2.0.CO;2)
- Jourdain, N. C., P. Marchesiello, C. E. Menkes et al. (2011), Mesoscale Simulation of Tropical Cyclones in the South Pacific: Climatology and Interannual Variability, *J. Climate*, 24, 3–25, doi: 10.1175/2010JCLI3559.1.
- Jullien, S., P. Marchesiello, C. E. Menkes, J. Lefèvre, N. C. Jourdain, G. Samson and M. Lengaigne (2014), Ocean feedback to tropical cyclones: Climatology and processes, *Clim. Dyn.*, 43, 9–10, 2831–2854.
- Jung, T., and Coauthors (2012), High-resolution global climate simulations with the ECMWF model in Project Athena: Experimental design, model climate, and seasonal forecast skill, *J. Climate*, 25, 3155–3172.
- Kain, J. S. (2004), The Kain-Fritsch convective parameterization: An update, *J. Appl. Meteorol*, 43, 1, 170–181, doi:10.1175/1520-0450(2004)043<0170:TKCPAU>2.0.CO;2.
- Karim, M. F., and N. Mimura (2008), Impacts of climate change and sea-level rise on cyclonic storm surge floods in Bangladesh, *Glob. Environ. Chang.*, 18, 3, 490–500.
- Knaff, J.A., and C.R. Sampson (2009), Southern Hemisphere tropical cyclone intensity forecast methods used at the Joint Typhoon Warning Center Part II: Statistical–dynamical forecasts, *Aust. Meteor. Oceanogr. J.*, 58, 9–18.
- Knaff, J.A., C.R. Sampson and M DeMaria (2005), An operational Statistical Typhoon Intensity Prediction Scheme for the western North Pacific, *Wea. Forecasting*, 20, 688–699.

- Knapp, K. R., M. C. Kruk, D. H. Levinson, H. J. Diamond and C. J. Neumann (2010), The International Best Track Archive for Climate Stewardship (IBTrACS): Unifying Tropical Cyclone Data, *Bull. Amer. Meteor. Soc.*, 10, doi:10.1175/2009BAMS2755.1.
- Lengaigne, M., S. Neetu, G. Samson, J. Vialard, K.S Krishnamohan, S. Masson, S. Jullien, I. Suresh, and C. E. Menkes (2017), Influence of air-sea coupling on Indian Ocean Tropical Cyclones, *Clim. Dyn.*, doi:0.1007/s00382-018-4152-0.
- Li, Z., W. Yu, T. Li, V. S. N. Murty, and F. Tangang (2013), Bimodal character of cyclone climatology in Bay of Bengal modulated by monsoon seasonal cycle, *J. Clim.*, 26, 1033-1046.
- Madec, G. (2008), NEMO ocean engine, *Note du Pôle de modélisation, Institut Pierre-Simon Laplace (IPSL)*, France, 27, ISSN No 1288-1619.
- Madsen, H., and F. Jakobsen (2004), Cyclone induced storm surge and flood forecasting in the northern Bay of Bengal, *Coastal Eng.*, 51, 277–296.
- Manganello J. V., and Coauthors (2012), Tropical cyclone climatology in a 10-km global atmospheric GCM: Toward weather-resolving climate modeling. *J. Climate*, 25, 3867-3893.
- McCreary, J. P., W. Han, D. Shankar, and S. R. Shetye (1996), Dynamics of the East India Coastal Current. 2. Numerical solutions, *J. Geophys. Res.*, 101, 13,993–14,010, doi:10.1029/96JC00560.
- Merrill R. T. (1988), Environmental influence of hurricane intensification, *J. Atmos. Sci.*, 45, 1678–1687.
- Murakami H et al (2015) Simulation and prediction of category 4 and 5 hurricanes in the high-resolution GFDL HiFLOR coupled climate model. *J Clim* 28(23):9058–9079. <https://doi.org/10.1175/JCLI-D-15-0216.1>
- Needham, H. F., B. D. Keim, and D. Sathiaraj (2015), A review of tropical cyclone-generated storm surges: Global data sources, observations, and impacts, *Rev. Geophys.*, 53, 545–591, doi:<https://doi.org/10.1002/2014RG000477>.
- Neetu, S., M. Lengaigne, E. Vincent, J. Vialard, G. Madec, G. Samson, M. R. Rameshkumar, and F. Durand (2012), Influence of upper ocean stratification on tropical cyclone-induced surface cooling in the Bay of Bengal, *J. Geophys. Res.*, 117, doi:10.1029/2012JC008433.
- Neetu, S.**, M. Lengaigne, H. B. Menon, J. Vialard, M.M. Ali, I. Suresh, C.E. Menkes, and J.A. Knaff (2017), Global assessment of statistical-dynamical prediction of tropical cyclones intensity, *QJRM*S, 143, 2143-2156, doi:10.1002/qj.3073.
- Ogata T, Mizuta R, Adachi Y, Murakami H, Ose T (2015) Effect of air–sea coupling on the frequency distribution of intense tropical cyclones over the northwestern Pacific. *Geophys Res Lett* 42:10415–10421. <https://doi.org/10.1002/2015GL066774>
- Pielke, Jr. R.A., J. Gratz, C. W. Landsea, D. Collins, M. A. Saunders, and R. Musulin (2008), Normalized hurricane damage in the United States: 1900–2005, *Nat. Hazards Rev.*
- Price JF (1981) Upper ocean response to a hurricane. *J Phys Oceanogr* 11:153–175. [https://doi.org/10.1175/1520-0485\(1981\)011<0153:UORTAH>2.0.CO;2](https://doi.org/10.1175/1520-0485(1981)011<0153:UORTAH>2.0.CO;2)

- Samson, G., S. Masson, M. Lengaigne, M. G. Keerthi, J. Vialard, S. Pous, G. Madec, N. C. Jourdain, S. Jullien, C. Menkes, P. Marchesiello (2014), The NOW regional coupled model: application to the Tropical Indian ocean climate and tropical cyclone activity, *J. Adv. Mod. Earth Sys.*, 6, 3, 700-722, doi:10.1002/2014MS000324.
- Satoh, M., K. Oouchi, T. Nasuno. and Coauthors (2012), Intra-seasonal oscillation and its control of tropical cyclones simulated by high-resolution global atmospheric models, *Clim. Dyn.*, 39, 2185, doi:10.1007/s00382-011-1235-6.
- Schade LR (2000) Tropical cyclone intensity and sea surface temperature. *J. Atmos. Sci.* 57:3122–3130. [https://doi.org/10.1175/15200469\(2000\)057<3122:TCIASS>2.0.CO;2](https://doi.org/10.1175/15200469(2000)057<3122:TCIASS>2.0.CO;2)
- Sengupta, D., R. G. Bharath, D. S. Anitha (2008), Cyclone-induced mixing does not cool SST in the post-monsoon north Bay of Bengal, *Atmos. Sci. Let.*, 9, 1-6.
- Shenoi, S. S. C., D. Shankar, and S. R. Shetye (2002), Differences in heat budgets of the near-surface Arabian Sea and Bay of Bengal: Implications for the summer monsoon, *J. Geophys. Res.*, 107(C6), 3052, doi:10.1029/2000JC000679.
- Skamarock, W. C., and JB Klemp (2008), A time-split nonhydrostatic atmospheric model for weather research and forecasting applications, *J. Comput. Phys.*, 227, 7, 3465-3485, doi:10.1016/j.jcp.2007.01.037.
- Valcke, S. 2013, The OASIS3 coupler: A European climate modelling community software, *Geosci. Model Dev.*, 6(2), 373–388, doi:10.5194/gmd-6-373-2013.
- Vincent EM, Lengaigne M, Madec G, Vialard J, Samson G, Jourdain N, Menkes CE, Jullien S (2012a) Processes setting the characteristics of sea surface cooling induced by tropical cyclones. *J. Geophys. Res.*, 117:C02020. <https://doi.org/10.1029/2011JC007396>
- Vincent EM, Lengaigne M, Vialard J, Madec G, Jourdain N, Mas- son S (2012b) Assessing the oceanic control on the amplitude of sea surface cooling induced by tropical cyclones. *J Geophys Res* 117:C05023. <https://doi.org/10.1029/2011JC007705>
- Xing, W., and F. Huang (2013), Influence of summer monsoon on asymmetric bimodal pattern of tropical cyclogenesis frequency over the Bay of Bengal, *Journal of Ocean University of China*, 12, 2, doi: 10.1007/s11802-013-2219-4.
- Yanase, W., M. Satoh, H. Taniguchi, and H. Fujinami (2012), Seasonal and intraseasonal modulation of tropical cyclogenesis environment over the Bay of Bengal during the extended summer monsoon. *J. Climate*, 25, 2914–2930.

Figure Captions

Figure 1. (a) Climatological distribution of normalised TC density (i.e. % of the total occurrence rate at each location) for observations (color) and CPL simulation (contour). (b) Climatology of the fraction of TCs that occur at a given month in the BoB for observations (red bars) and CPL (blue bars). The two shaded regions highlight the pre- and post-monsoon TC seasons definitions used in this paper. Composite evolution of the SST cooling within 200 km of all TCs in the BoB (in °C) during the (c) pre- and (d) post-monsoon for observations (red) and CPL simulation (blue). The whiskers on panels (b), (c) and (d) display the 90% confidence intervals based on a bootstrap method.

Figure 2. Percentage of BoB TCs as a function of their mean wind intensity during the pre- (green) and post-monsoon (blue) for (a) observations, (b) CPL and (c) FOR simulations. The inset indicates the overall percentage of intense TCs (defined as Category 2 and above). The whiskers display 90% confidence intervals based on a bootstrap method.

Figure 3. (a) Pre- minus post-monsoon BoB-averaged maximum potential intensity (MPI), relative humidity at 600hPa (RH) and vertical wind shear (SHEAR) in % for ERA-I (red), CPL (blue) and FOR (green). (b) Percentage of BoB intense TCs (category 2 and above) for CPL and FOR during the pre and post-monsoon. The whiskers display 90% confidence intervals based on a bootstrap method.

Figure 4. Mean inner-core (i.e. within 200 km of the TC centre) (left panels) SST, (middle panels) upward surface enthalpy flux and (right panels) TC intensification rate as a function of the TC maximum wind speed for intensifying BoB TCs in (upper panels) FOR and (lower panels) CPL during the pre- (green) and post-monsoon (blue). This figure was obtained through averaging within 5 ms^{-1} TC maximum wind bins. The intensification rate is calculated as a centered difference using the TC maximum wind speed 12 hours before and after any given time.

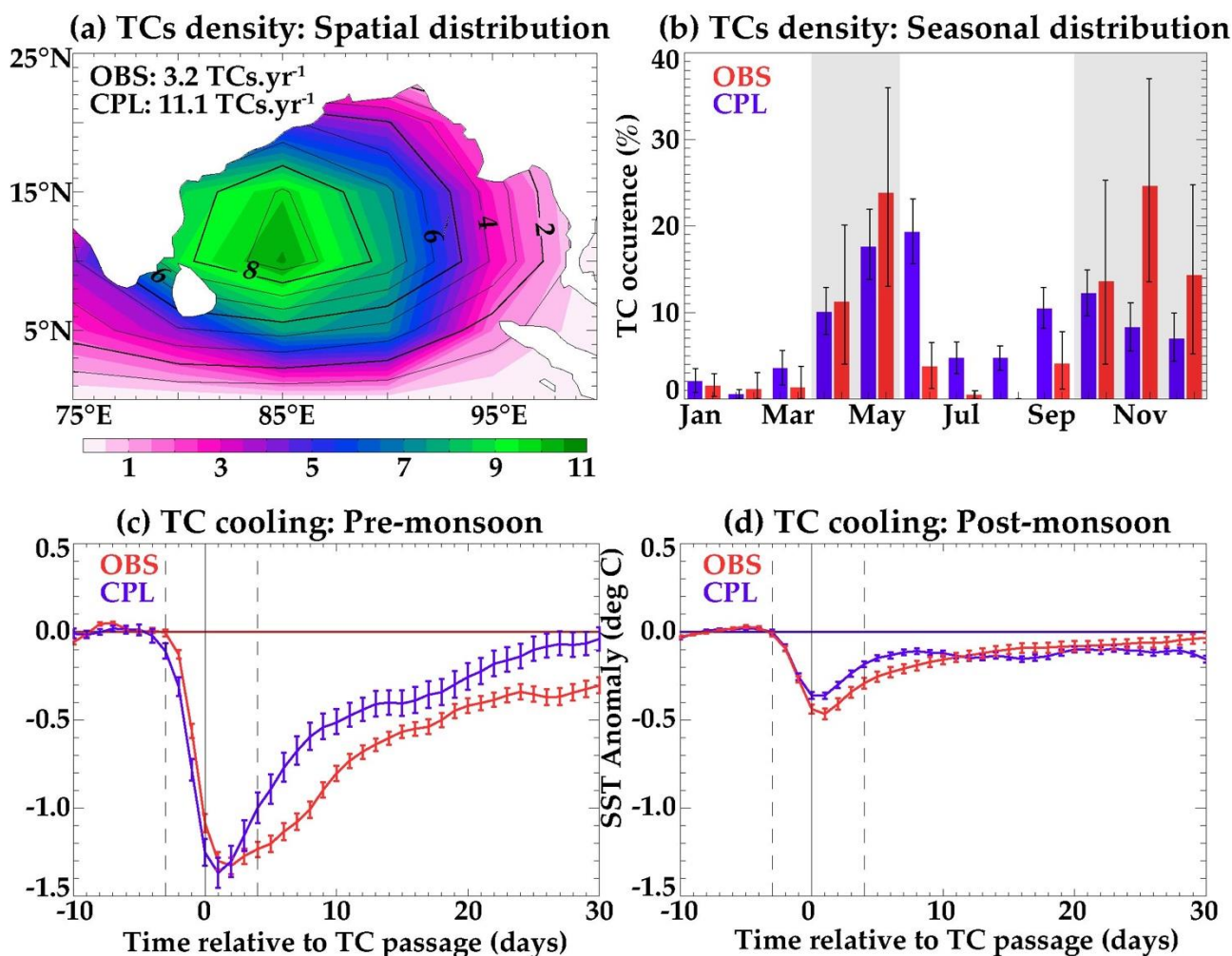


Figure 1. (a) Climatological distribution of normalised TC density (i.e. % of the total occurrence rate at each location) for observations (color) and CPL simulation (contour). (b) Climatology of the fraction of TCs that occur at a given month in the BoB for observations (red bars) and CPL (blue bars). The two shaded regions highlight the pre- and post-monsoon TC seasons definitions used in this paper. Composite evolution of the SST cooling within 200 km of all TCs in the BoB (in °C) during the (c) pre- and (d) post-monsoon for observations (red) and CPL simulation (blue). The whiskers on panels (b), (c) and (d) display the 90% confidence intervals based on a bootstrap method.

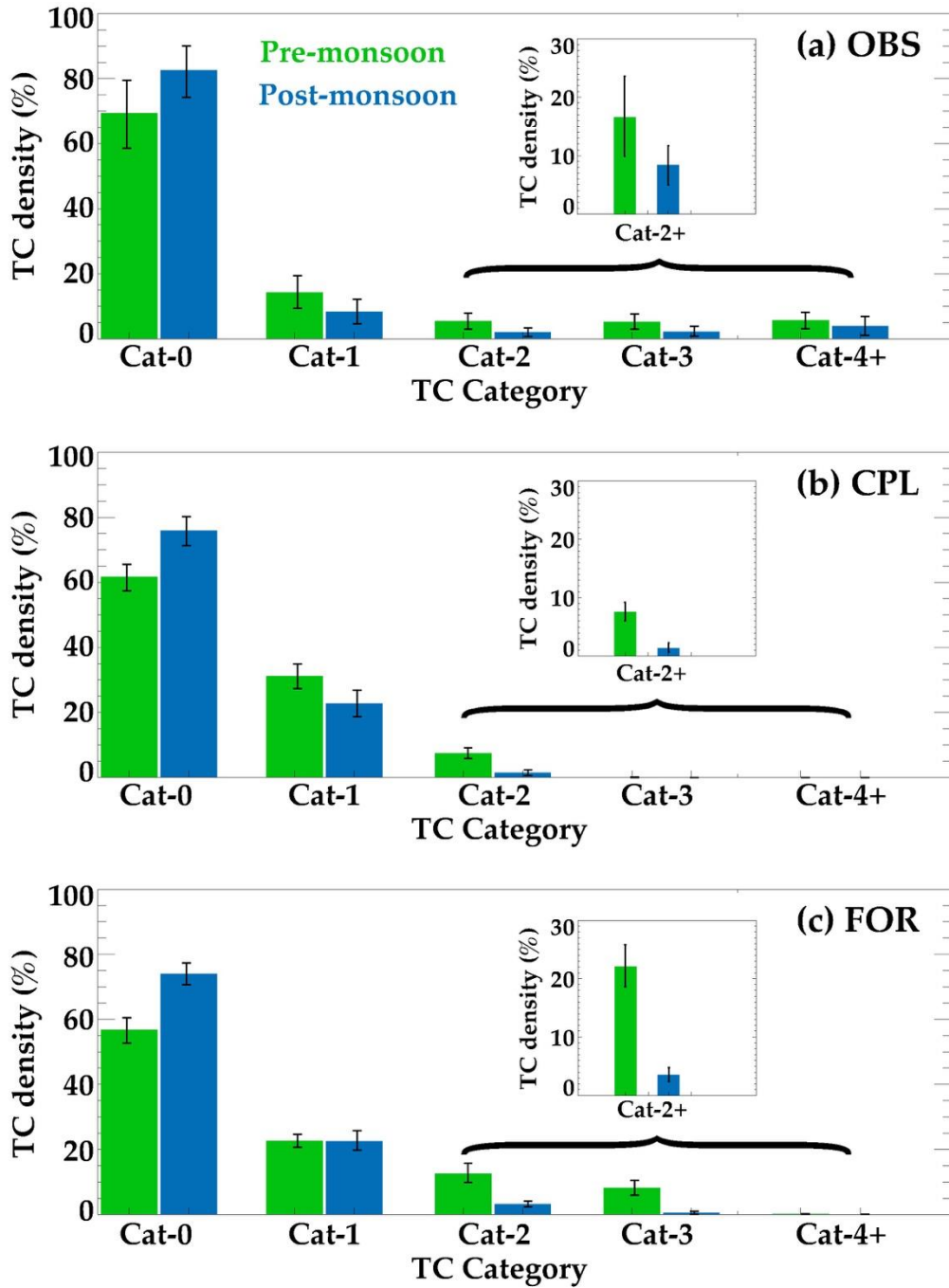


Figure 2. Percentage of BoB TCs as a function of their mean wind intensity during the pre- (green) and post-monsoon (blue) for (a) observations, (b) CPL and (c) FOR simulations. The inset indicates the overall percentage of intense TCs (defined as Category 2 and above). The whiskers display 90% confidence intervals based on a bootstrap method.

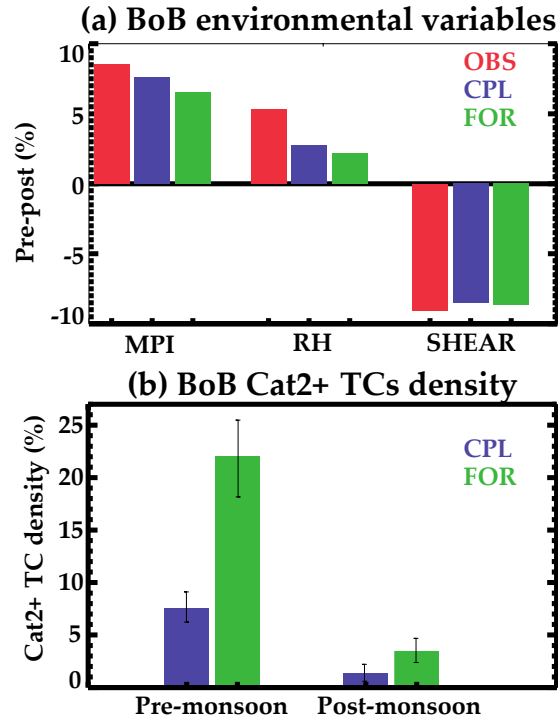


Figure 3. (a) Pre- minus post-monsoon BoB-averaged maximum potential intensity (MPI), relative humidity at 600hPa (RH) and vertical wind shear (SHEAR) in % for ERA-I (red), CPL (blue) and FOR (green). (b) Percentage of BoB intense TCs (category 2 and above) for CPL and FOR during the pre and post-monsoon. The whiskers display 90% confidence intervals based on a bootstrap method.

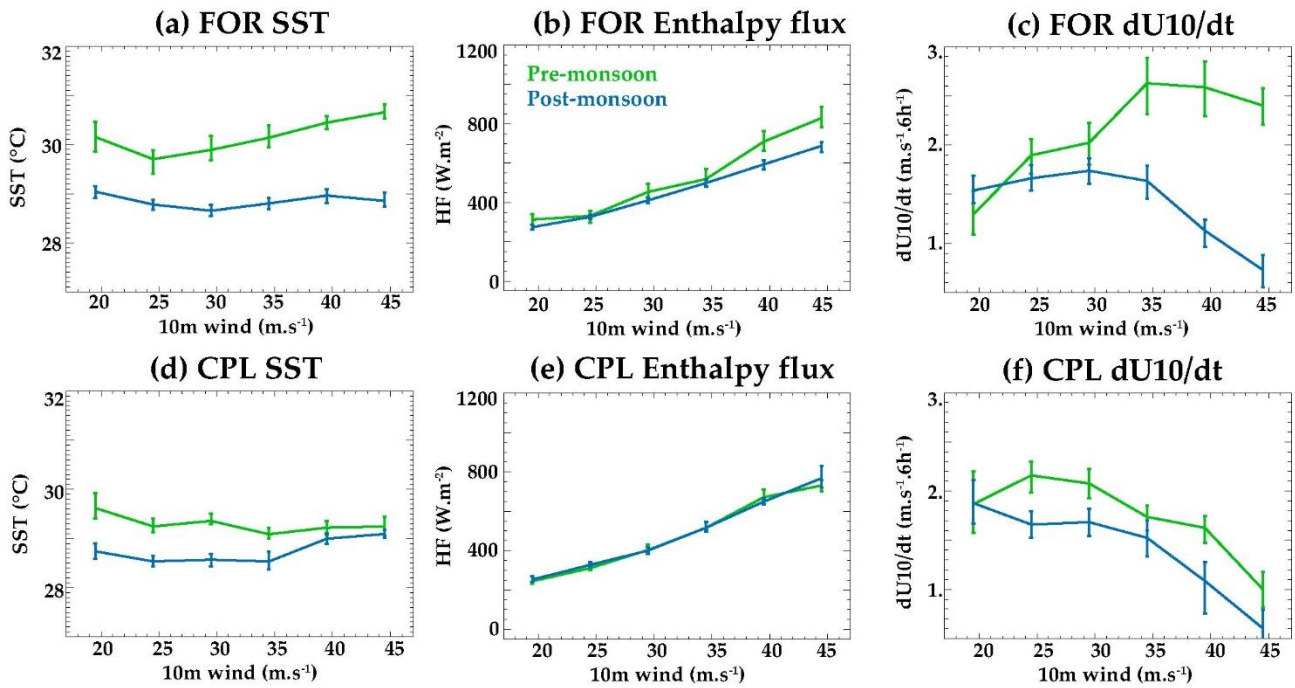


Figure 4. Mean inner-core (i.e. within 200 km of the TC centre) (**left panels**) SST, (**middle panels**) upward surface enthalpy flux and (**right panels**) TC intensification rate as a function of the TC maximum wind speed for intensifying BoB TCs in (**upper panels**) FOR and (**lower panels**) CPL during the pre- (green) and post-monsoon (blue). This figure was obtained through averaging within 5 ms⁻¹ TC maximum wind bins. The intensification rate is calculated as a centered difference using the TC maximum wind speed 12 hours before and after any given time.